Biochimica et Biophysica Acta 1850 (2015) 759–768

Contents lists available at ScienceDirect

Biochimica et Biophysica Acta

journal homepage: www.elsevier.com/locate/bbagen

Vertical ordering sensitivity of solid supported DPPC membrane to alamethicin and the related loss of cell viability

F. Domenici [a,b,*], F. Dell'Unto [b], D. Triggiani [c], C. Olmati [d], C. Castellano [e], F. Bordi [a,f,g], A. Tiezzi [c], A. Congiu [a]

[a] Dipartimento di Fisica, Università Sapienza, P.le A. Moro 5, 00185 Roma, Italy
[b] Dipartimento di Scienze e Tecnologie Chimiche, Università di Roma Tor Vergata, Via della Ricerca Scientifica 1, 00133 Roma, Italy
[c] Dipartimento per l'Innovazione dei sistemi Biologici, Agroalimentari e Forestali, Università degli Studi della Tuscia, Via San Camillo de Lellis s.n.c., 01100 Viterbo, Italy
[d] Banca del Germoplasma della Tuscia, Università degli Studi della Tuscia, Largo dell'Università s.n.c., 01100 Viterbo, Italy
[e] Dipartimento di Chimica, Università degli Studi di Milano, Via Golgi 19, 20133 Milano, Italy
[f] CNR-IPCF UOS Roma, Dipartimento di Fisica, Università Sapienza, P.le A. Moro 5, 00185 Roma, Italy
[g] Center for Life Nanoscience@Sapienza, Istituto Italiano di Tecnologia, V.le Regina Elena, 291, 00185 Rome, Italy

ARTICLE INFO

Article history:
Received 27 September 2014
Received in revised form 23 December 2014
Accepted 8 January 2015
Available online 15 January 2015

Keywords:
X-ray diffraction
Alamethicin
Lipid membrane
DPPC
HeLa cell
MTT assay

ABSTRACT

Background: Experimental studies of antimicrobial peptides interacting with lipid membranes recently attracted growing interest due to their numerous biomedical applications. However, the influence of such peptides on the structural organisation of lipid membranes in connection with the actual cell response still remains an elusive issue.
Methods: X-ray diffraction was employed on detecting the sensitivity of the periodical spacing of dipalmitoyl-phosphatidyl-choline stacked as solid-supported bilayers to the presence of varying amounts of the peptide alamethicin in a wide range of peptide-to-lipid molar ratios. These results were then correlated with the effects of alamethicin on biological membranes *in vitro* as observed by optical microscopy and microculture tetrazolium assay on the tumour cells *HeLa* to provide a comprehensive and quantitative analysis of these effects, based on a dose–response relationship.
Results: The experiments allowed correlating the periodical spacing and the peptide-to-lipid molar ratio on alamethicin-dipalmitoyl-phosphatidyl-choline samples. Two different trends of periodical spacing *vs.* peptide-to-lipid molar ratio clearly appeared at low and high hydration levels, showing intriguing non-linear profiles. Unexpected correspondences were observed between the peptide-to-lipid molar ratio range where the changes in dipalmitoyl-phosphatidyl-choline structure occur and the alamethicin doses which alter the viability and the plasma membrane morphology of *HeLa*.
Conclusions: Alamethicin might induce either mechanical or phase changes on dipalmitoyl-phosphatidyl-choline bilayers. Such easily accessible ordering information was well-calibrated to predict the alamethicin doses necessary to trigger cell death through plasma membrane alterations.
General significance: This benchmark combined study may be valuable to predict bioeffects of several antimicrobial peptides of biomedical relevance.

1. Introduction

It is well known that the amphipathic properties of the phospholipids in cell membranes characterise both the bilayer structural assembly and the interconnecting processes with the external environment. Analogously, there is an entire class of antimicrobial peptides that carry out their function by exhibiting a prominent amphipathic character, allowing for their insertion between both polar and hydrophobic groups of the phospholipids. This results in an increase in the membrane's permeability, as well as cell lysis. This behaviour was intensively investigated over the past few years [1–10].

Depending on the composition and concentration of peptides, they adsorb themselves either parallelly or perpendicularly to the lipid bilayer surface (mostly exhibiting α-helical folding), thus causing membrane thinning, pore formation, and even detergent-like effects [1–3]. Beside this, some antimicrobial peptides (*i.e.* Indolicin) have also shown additional cytotoxic activity promoted by the inhibition of DNA and protein synthesis [10].

An ever-growing body of research has focused on understanding the mechanisms of action of antimicrobial peptides against neoplastic cells [4–9]. According to these studies, antimicrobial peptides can cause cancer cell death through the direct disruption of the membranes, as evidenced in erythro-leukaemia [4], breast cancer [5] and synovial

* Corresponding author at: Dipartimento di Fisica, Università Sapienza, P.le A. Moro 5, 00185 Roma, Italy. Tel.: +39 0649913503.
E-mail address: fabiodomenici@gmail.com (F. Domenici).

http://dx.doi.org/10.1016/j.bbagen.2015.01.006
0304-4165/

sarcoma cell lines [6]. Some antimicrobial peptides (*i.e.* Lactoferricin B, β-hairpin peptides) can trigger regulated cell death through intracellular signalling mechanisms [5,9], which may involve the participation of intracellular calcium mechanisms [5], and of apoptosis by targeting the mitochondrial membranes [7–9]. Even if intracellular targets were involved, an initial cell membrane interaction with such peptides is required for cytotoxic activities, and this interaction determines the spectrum of target cells.

A quantitative analysis of the interaction of these antimicrobial peptides with natural cell membranes, due to their extreme complexity, is a very difficult task. Therefore, varied model assemblies have been employed to mimic the lipid bilayer organisation of the membrane [11–16]. These models include multilamellar and unilamellar liposomes, colorimetric biomimetic membranes, and planar lipid mono-, bi- and multi-layers deposited on solid supports.

The investigation of the self-assembled lipid bi- or multi-layer on solid support is particularly advantageous because it allows for the examination of the peptide-induced membrane ordering changes in relation to its own conformation [17,18] under several different physico-chemical conditions. In this study, we focused on the interaction between alamethicin (Ala) and a solid-supported membrane made up of the naturally occurring and well-studied saturated lecithin dipalmitoyl-phosphatidyl-choline (DPPC), under different hydration and temperature conditions [19].

Ala [20] is one member of the large family of antimicrobial peptides characterised by the presence of non-proteinogenic amino acids in the primary structure (mostly alfa-aminoisobutyric acid and isovaline), a C-terminal amino alcohol and an acylated N-terminal group. The biological activity of Ala is likely due to its ability to form water-filled channels in lipid membranes [18,21–26] (see also, Section 3). Its structural conformation strongly depends on the peptide/lipid molar ratio (*P/L*), the hydration/humidity level and the temperature. At low *P/L*, Ala preferentially adsorbs to the membrane's surface, where it is aligned with its N-terminal residue that is partially buried in the hydrophobic region of the lipid layer. Simultaneously, the C-terminal is hydrogen-bonded to the water molecules surrounding the lipid headgroups [24,26]. With increasing peptide concentrations, its rearrangement results in its insertion into the membrane. Above a certain critical *P/L* value, nearly all peptide molecules participate in the formation of hydrophilic pores [18,22,23]. Such pores, by conducting water and ionic species, can cause cell death by altering the osmotic balance [21]. Since the channel activity shows discrete multilevel conductances [25], a barrel stave model has been suggested for its structure [27,28].

DPPC is an abundant and common structural plasma membrane lipid implicated in forming biologically relevant separate lipid phases [29]. Depending on temperature, DPPC bilayers exhibit three different structures of biological interest, namely a gel phase (L_β) ($T < 35$ °C), with an overall ordered hydrocarbon chain arrangement, a liquid-crystalline phase (L_α) ($T \geq 42$ °C) and a ripple phase (P_β) ($35 \leq T < 42$ °C). It was recently suggested that Ala insertion into the membranes might also influence the chain melting transition of such lipid layers [30–32]. In fact, from calorimetric studies [30–32], the gel-to-fluid transition profiles appeared to be broadened and had shifted in temperature from the addition of Ala into the DPPC membranes. Atomic Force Microscopy and freeze–fracture studies [32,33] gave further support to this hypothesis, both showing alterations, at the nano-scale, of the lipid ordering in the vicinity of the peptide pores. All of these findings have been discussed in terms of the ability of Ala pores to promote structural gel–liquid-crystalline, as well as gel–ripple mesophase [33,34] transitions in the DPPC bilayers. However, to our knowledge, this hypothesis still lacks convincing evidence.

The latter scenario reinforces the need to follow the ordering behaviour of the lipid membrane embedded with Ala in the broadest concentration range of biological relevance. This is especially true if the structural information achieved on model membranes were to be exploited as an easy way to explain and predict the cytotoxicity of Ala that has been triggered by either mechanical or phase alterations of the lipid assembly composing the biological membranes.

The energy dispersive X-ray diffraction (EDXD) applied to the solid supported lipid membranes allowed for an accurate monitoring of the conformational changes, since small alterations in the lamellae periodicity also unequivocally correlate with lipid structural phase changes. In a previous work [18], we highlighted the huge potential of the EDXD method to figure out the effects of Ala on a liquid-crystalline lipid membrane made up of dioleoylphosphatidylcholine that retains stability in its liquid-crystalline phase.

In the present work, we employed this powerful technique to gain hints on the role of Ala in the vertical ordering of the solid supported gel-crystalline DPPC layers, the latter being susceptible to also change the equilibrium of thermo-lyotropic mesophase [32–35]. To this aim, in our experiments, we varied the peptide/lipid molar ratio over a wide range using two different hydration levels.

The biological relevance of this investigation clearly appeared if the obtained EDXD results were compared with the *in vitro* tests performed on the carcinoma *HeLa* cell line. Effects of Ala on cell viability and plasma membrane morphology were screened in terms of dose and time of exposure. They were also intersected with the equivalent *P/L* range that affects the vertical ordering of the DPPC layers. The *in vitro* cytotoxic effect of Ala that was reported might also provide some hints on the peptide interaction with cancer cells.

2. Material and methods

2.1. Peptide–lipid preparation

Alamethicin was purchased from Sigma-Aldrich Chemical (St. Louis, MO). The Sigma product was a mixture of alamethicin I (85% by high-performance liquid chromatography) and alamethicin II (12%), differing by one amino acid. Silicon wafers (1 1 0) (30 mm × 40 mm × 0.15 mm) were purchased from ACM (Villiers St. Fredric, France). The silicon's surface was thoroughly cleaned using 2-propanol and 1,1,1-trichloroethane to remove hydrophilic and hydrophobic contaminants, respectively. A nitrogen flux was used to remove any trace of solvent. The peptide/lipid mixtures at the desired molar ratios were first dissolved in a 1:1 (v/v) trifluoroethanol–chloroform solvent, and were then uniformly deposited onto a recently cleaned silicon substrate. After slowly evaporating the solvent in air, we obtained a film coating that appeared smooth and uniform to the naked eye. The film was kept under vacuum for 24 h to promote further release of residual solvent molecules [36]. It was then hydrated with saturated water vapour (100% RH) and incubated for 24 h. The full-hydration of samples was thus attained by avoiding their immersion within the bulk liquid water, the latter being the cause of significant alteration/detachment of the amphipathic peptide–lipid film from the silicon support, as well as of suppression/distortion effects of the X-ray signal. We checked the homogeneity of the film by performing diffraction measurements at different sample positions. As deduced from the Bragg peak (see the Scherrer equation in the next section), in all of the experiments, the DPPC films appeared to be roughly formed by at least ≈15 double layers.

Our samples were prepared at 10 different peptide/lipid (*P/L*) molar ratios (ranging from 0 to 1, see Table 1). During the X-ray measurements, the sample was kept inside a controlled humidity–temperature chamber at $T = 25$ °C, where the bare DPPC was in the L_β phase. The influence of water hydration on the vertical ordering of the Ala-DPPC films was investigated by choosing two RH environmental conditions: at 50% RH, the membrane underwent dehydration down to the thermodynamic equilibrium, ensuring, in turn, that only a small number of water molecules remained absorbed onto the polar membrane surface [13]; at 100% RH, the membrane could instead reach the maximum amount of adsorbed water [13]. In all of the experiments, Milli-Q quality water was employed (18.2 MΩ cm, resistivity).

Table 1
Periodicity *d* (with peak width *w*, from Gaussian fit) pointed out by EDXD at 25 °C on silicon supported membranes made up of Ala-DPPC at varying *P/L*, and at different percentages of RH environment. Pure DPPC samples are referred to $P/L = 0$.

P/L	0	0.00313	0.00625	0.0125	0.01667	0.025	0.03333	0.05	0.1	1
d [Å] 50% RH	62.5	62.0	61.6	59.9	57.7	56.5	57.6	60.0	60.8	–
d [Å] 100% RH	65.8	65.3	64.7	64.7	64.7	64.7	64.5	66.6	67.4	64.4
w [$Å^{-1}$] 50% RH	0.00612	0.00793	0.01134	0.01104	0.01118	0.00707	0.01115	0.01165	0.01024	–
w [$Å^{-1}$] 100% RH	0.00735	0.00735	0.00751	0.00801	0.00969	0.01000	0.00726	0.0099	0.01121	0.00832

2.2. Energy dispersive X-ray diffraction

X-ray diffraction experiments were performed with a home-built energy dispersive X-ray diffraction (EDXD) apparatus using a small angle configuration [37,38]. Briefly, the Bremsstrahlung radiation of a tungsten anode tube with two beryllium windows for long line focus of 0.4×12 mm, and operating at 50 kV and 40 mA, was used as a source (Thomson). The diffracted beam was energy-resolved by an EG&G (ORTEC, Oak Ridge, TN) liquid-nitrogen-cooled ultrapure germanium solid-state detector. The apparatus operated in conventional Bragg–Brentano θ–θ geometry (where θ is the angle between the X-ray source and the sample), with the two arms rotating in the vertical plane along the same axis centred on the sample, which remained horizontal during the entire measurement. In this geometry, the diffraction vector *Q* was always normal relative to the sample's surface. Different scattering angles were used to study the selected range of the reciprocal space. The uncertainty associated with θ was $\Delta\theta = 0.001°$ and the energy resolution was ca. 1% with a maximum count rate of 10 kcounts/s. The energy of diffracted photons, E, at the grazing incident angle θ was related to the reciprocal vector *Q* by the Bragg's relationship $Q = 4\pi/(hc)\ E \sin\theta$; (h and c are as usual the Plank constant and the speed of light in the vacuum, respectively). The diffraction patterns were acquired at $\theta = 0.350°$. At this small angle, the contribution of incoherent scattering from the sample was negligible, and allowed for acquiring contemporaneously detailed broadband patterns (2000 s, live time; 5% dead time), including the first three order Bragg peaks (see also Section 4.1), without changing the irradiated sample area.

The patterns were fitted to a Gaussian model (OriginLab software) to obtain the lamellar periodicity (periodical spacing or repeat distance) from the position of the first order Bragg peak through the relation $d = 2\pi/Q$, where *Q* is the mean (central) value of the Gaussian fit. The full width at half maximum (*w*) of a Bragg peak was related to the inverse of the number of coherent scattering domains *N* within the lipid assembly, which in turn, reflected the number of lipid bilayers formed, through the relation (named Scherrer equation) $w = 0.9 \cdot 2\pi/(N \cdot d)$. It is moreover affected by the presence of structural defects, non-uniform strains, thermal fluctuations and roughness of the sample and, therefore it is usually associated with the ordering grade of samples.

For all of the measurements, a custom homemade sample cell was used allowing for the acquisition of measurements in a wide range of temperatures (from −40 °C to 120 °C), pressures (down to 10^{-3} mbar) and relative humidity (RH) (up to 100%) conditions.

The RH level was checked by a digital hygrometer (2%, RH accuracy). The temperature of the wafers was accurately varied and monitored by using a fuzzy logic digital controller (West 6400) equipped with a mini tubular heater and a Pt100 probe (0.1 °C, T accuracy). The cooling and heating rates were controlled at 0.2 °C per minute. Thermal equilibrium and full hydration conditions of the samples were assessed by means of low-statistic preliminary measurements at regular time intervals.

2.3. Cell culture

HeLa cells derived from *human cervix adenocarcinoma* were purchased from American Type Culture Collection (ATCC CCL-2.2). This cell line was maintained in DMEM (Sigma), supplemented with 10% heat-inactivated foetal bovine serum (Sigma-Aldrich) and 100 IU/ml of penicillin and streptomycin. The cells were kept incubated at 37 °C under 5% CO_2. The cultures were grown in 75 cm^2 tissue culture flasks containing 10 ml of medium, which were replaced three times per week. Stock cultures were split into new flasks once every seven days. Approximately cell monolayers at 95% confluence were used for the experiments.

2.4. Cytotoxic assay

HeLa (100,000 cells/cm^2) were seeded in 96-well microplates in growth medium (100 μl/well) and then incubated at 37 °C in under 5% CO_2. After 20 h, the medium was removed and replaced with 50-μl of fresh medium containing the compound to be studied at the appropriate concentrations.

Three different treatment procedures were carried out:

a) Two hours of treatment by addition of alamethicin ranging from 1.25 to 50 μg/ml;
b) Six hours of treatment by addition of alamethicin ranging from $2.5 \cdot 10^{-4}$ to 2.0 μg/ml;
c) 20 h of treatment by addition of alamethicin ranging from $3.0 \cdot 10^{-4}$ to 1.0 μg/ml.

The living cell activity was measured using the MTT [3-(4,5-dimethylthiazol-2-yl)-2,5-diphenyltetrazolium bromide] assay, a colorimetric method of measuring the activity *via* mitochondrial dehydrogenases.

After incubation with the tested substance (2 h of treatment, "a"; 6 h of treatment, "b"; 20 h of treatment, "c"), 10 μl of a MTT solution was added to each well. Then, the cells were further incubated for 4 h at 37 °C. The blue MTT-formazan product was solubilised by the addition of 100 μl of DMSO and the absorbance was measured at 595 nm using a Victor III spectrophotometer. The cytotoxic activity was calculated as a percentage of remaining viable cells *versus* control (untreated cells) conditions. The results for each experimental condition are presented as the mean ± standard deviation of the 16 replicate wells. Statistical comparisons were made using Tukey's test.

2.5. Light microscope

Cell morphology was observed and photographed using a NIKON microscope (Eclipse TS100) with a 40× objective. Photo images from videotapes were obtained using the software Studio9.

3. Theoretical background

3.1. Ala/lipid membrane interplay: elasticity model and hydrophobic interaction

The crystal structure of Ala was solved more than 20 years ago using X-ray crystallography. The amphipathic peptide is active, forming membrane defects in some cells but not in others, so that it could function as host–defence agent, killing infectious microbes. The process of pore-like defect formation is thought to be promoted by a combination of

different interactions of the peptide residues with the lipid molecules, *i.e.*, electrostatic ones with the lipid polar heads and hydrophobic ones with the acyl chains. The structure of Ala pores is generally described in terms of the "barrel-stave" model, where multiple peptide molecules form a helix bundle surrounding a central pore. In addition, since pores do not appear until the rupture tensions of lipid membrane occur, Ala can also be considered a mechanosensitive peptide [39].

As Chen et al. [23,40] demonstrated, as long as the peptide lipid ratio P/L was smaller than the lipid-dependent threshold value $(P/L)^*$, Ala molecules adsorb on the membrane lying flat on its surface (*i.e.* with the axis of the helical peptides oriented parallel to the bilayer). However, as P/L overcame $(P/L)^*$, an increasing fraction of peptides changed orientation, becoming perpendicular to the bilayer. Below $(P/L)^*$, the bilayer thickness decreased linearly with P/L, levelling off after P/L exceeded $(P/L)^*$. The same authors proposed a model (hereafter, *elasticity model*) [23] that was able to effectively describe these findings. The basic idea was that when a peptide adsorbs on the bilayer, it causes a local expansion of membrane area. Due to the volume conservation of the hydrocarbon chains, such expansion in the area (ΔA) must be compensated for by a thinning ($-\Delta d$) of the bilayer thickness, d. In fact, to have $\Delta V \approx 0$, at a first approximation, $\Delta A/A$ must be $\approx \Delta d/d$.

By writing the linear relationship between $\Delta d/d$ and the molar ratio P/L as

$$-\Delta d/d \approx \Delta A/A = (A_P/A_L)\,(P/L), \quad (1)$$

the angular coefficient of the slope of a plot of $-\Delta d/d$ *versus* P/L provided the value of the A_P/A_L ratio, where A_L is the cross-section area per lipid and A_P is the area increase caused by one peptide [18]. Within the elasticity model, such thinning was assumed to be associated with an internal membrane tension. Then, the introduction in the free energy of the system of two different tension terms, for the parallel and vertical orientations of the peptide, led to a relation that was able to explain the observed P/L-dependence and the existence of a threshold value [23,40].

More recently, it was proposed that in addition to elastic contributions, lipid mediated forces controlling the peptide partitioning within the lipid membrane could be described in terms of "hydrophobic mismatch". In particular, since Ala formed barrel-stave pores, an additional thinning effect could be due to a hydrophobic mismatch between the hydrophobic region of the Ala helix and the hydrocarbon region of the lipid bilayer [22,41,42]. Generally the hydrophobic length of the Ala helix is different, mostly shorter than the hydrocarbon thickness of the lipid bilayers and the interaction between amphipathic peptides and lipids would depend on the relative length difference of their hydrophobic cores [22]. In fact, hydrophobic mismatch can have large effects on the structural features of the lipid assembly [32,43–45]. In their "mattress model", Mouritsen and Bloom [44] suggested that hydrophobic mismatches of membrane peptides and phospholipid structures could induce changes in the membrane thickness and ordering caused by both stretching and disordering the lipid acyl chains composing the involved membrane bilayer.

Finally, an influence of Ala on the chain melting transition of the lipid membrane, and in turn, on its equilibrium mesophase structure, was recently inferred [31]. In line with this, variations in lamellar spacing of biomembranes may hide perturbation in phase equilibria and hydrophobic mismatching, both playing a pivotal role in transmembrane protein sorting and biological function [46].

4. Results and discussion

In this section, we report on the EDXD analysis of vertical ordering of solid supported Ala-DPPC film at varying P/L molar ratios and hydration levels. Then, we show alterations of viability and morphology disclosed on *HeLa* cells, thus evaluating the consistence between significant changes observed on DPPC membranes and *in vitro*.

4.1. EDXD measurements

We collected EDXD patterns on several different regions of partially (50% RH, 25 °C) and fully (100% RH, 25 °C) hydrated samples made up of DPPC and Ala-DPPC films self-assembled on silicon wafers, as described in Section 2.1. Representative profiles are shown in Fig. 1 and 2, together with Gaussian fit. The analysis of the patterns in terms of Gaussian spectral lines pointed out that the experimental profiles were essentially a superposition of the first order Bragg peaks, reflecting the period of the stacks of lamellar bilayers. The corresponding Q (reciprocal d-spacing) and width (w) are listed in Table 1. Upon a long acquisition time, the diffraction patterns of the fully hydrated samples also exhibit weakly intense second and third order Bragg peaks (see the inset of Fig. 2), which rapidly vanish as the Ala/DPPC molar ratio increases. As expected [47–50], the w value of Ala-DPPC samples, subjected to both a constant 50 and a 100% RH, increased accordingly, thus confirming that the presence of Ala significantly affects the order degree of the DPPC assembly.

As can be easily calculated from Table 1 (see also Section 2.2), for a pure DPPC membrane exposed to the saturated water vapour condition (RH increased from 50 to 100%), the periodicity d increased from 62.5 ± 0.5 Å to 65.8 ± 0.5 Å. This result was in agreement with previous findings on water-dispersed vesicles, as well as on oriented films laid on different substrates [51,52]. This means that the ordering and the lyotropic behaviour of the DPPC membrane were not significantly affected by the particular deposition method employed.

At 50% RH, Fig. 1 shows that the mean value of the Bragg peak shifted monotonically in two opposite directions, depending on P/L ratio below and above a characteristic P/L value (≈0.025). This indicated that below this threshold, the DPPC membrane spacing underwent a thinning (Fig. 1a), while above this value, the layer thickness increased again (Fig. 1b).

At a much higher RH (Fig. 2, 100% RH), as P/L varied in the range of 0 to 0.1, a comparatively different phenomenology was observed. While, similarly to what was observed at the lower hydration condition, a significant d reduction was detected (from 65.8 ± 0.5 Å for pure DPPC down to the minimum value of 64.7 ± 0.5 Å) as P/L increased from 0 to 0.00625 (Fig. 2a). When P/L was further increased between 0.0125 and ≈0.0333, the spacing d remained constant (Fig. 2b), increasing again only for $P/L >$ ≈0.0333. It ultimately reached the value of 67.4 ± 0.5 Å at P/L= 0.1, which was larger than was the d value observed for pure DPPC (Fig. 2c).

The Ala-DPPC sample measured at $P/L = 1$, whose diffraction patterns at 50 and 100% RH environments are shown in Supplementary Data Fig. S1, earned separate attention. In practice, the EDXD profiles in Fig. S1 demonstrated that Ala-DPPC film at a high Ala concentration and a low hydration level exhibited a weak and broadened signal, in which the Bragg peak shape could be discerned only after a prolonged acquisition time was set. Interestingly, upon the same Ala-DPPC film that was treated under 100% RH, a first order Bragg peak could instead be clearly observed. Both Q and w, belonging to the latter Ala-DPPC lamellar structure (recovered by water), are also reported in Table 1 and were quite similar to those of samples highly hydrated at lower P/L ratios. The simulation supports a role for the local deformation of the phospholipid bilayer in the mechanism of peptide-induced membrane lysis. This may possibly occur in relation to the water penetration [41]. In this case, it was clear that to a high level of Ala concentration could follow a disruptive effect (often referred to as detergent effect) on lipid membranes, preventing the DPPC from multilayers assembly. On the other hand, the lipid–water interface was critical for the packing of lipid molecules into membranes [43]. Accordingly, the hydration (by the formation of hydrogen bonds between the water and the polar heads of the PC) would favour a long range ordering configuration, mainly in the lipid areas at lower Ala concentrations.

Fig. 3 shows the values of d as a function of P/L ($0 \div 0.1$), measured for the samples in the two conditions: 50 and 100% RH. At low values of

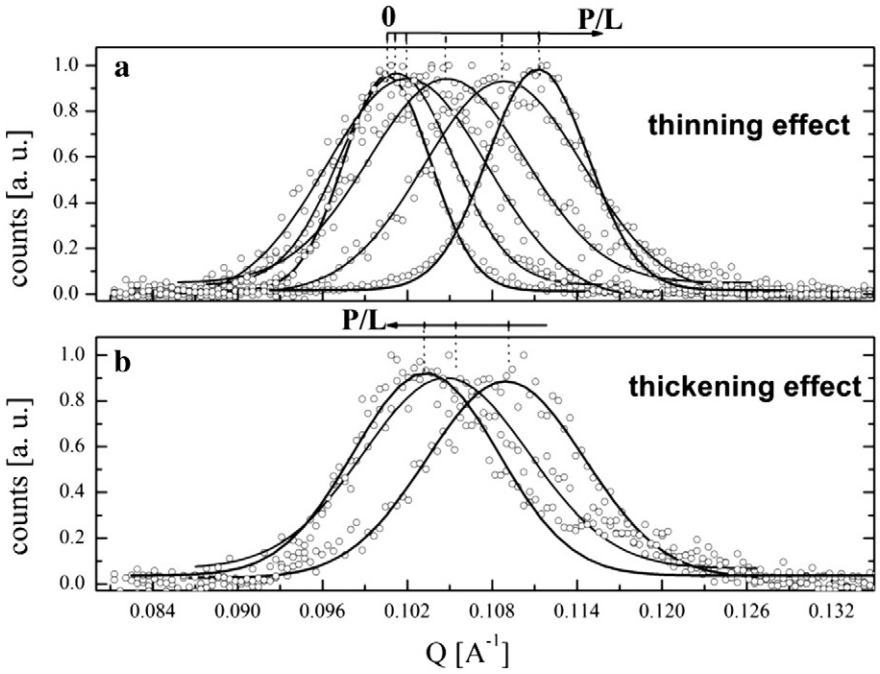

Fig. 1. First order Bragg peaks in reciprocal space of Ala-DPPC on silicon support at different values of *P*/*L* molar ratios, 25 °C and 50% RH are reported in scatter plot; corresponding best fit by Gaussian model in line plot. Panel a: For *P*/*L* ranging from 0 to 0.025, the higher the *P*/*L* value and the higher the mean *Q* value (the arrow marks the direction of the progressive shift of the peaks with *P*/*L*), indicating that the periodical spacing of DPPC undergoes a thinning effect. Panel b: When *P*/*L* overcomes 0.025 up to 0.1, the progressive shift of the mean *Q* value of the peaks with *P*/*L* proceeds in the opposite direction (see the arrow), indicating that the periodical spacing of DPPC undergoes a thickening effect.

P/*L* (0 ÷ 0.00625, *P*/*L*), a linear dependence of *d vs*. *P*/*L* was observed (Fig. 3), showing a non-significant difference in slope for both of the RH values explored. According to Lee et al. [22], this meant that within this range of *P*/*L* values, the helical peptides were embedded oriented parallel to the DPPC bilayer (see also Section 3). From the linear slope of $\Delta d/d$ *vs*. *P*/*L* (Eq. 1), the area increase A_P caused by the adsorption of one peptide could be calculated. With our experimental values, we obtained a value of 230 ± 20 Å^2 for A_P. This value was in good agreement with the X-ray crystallography Ala cross-section (corrected for approximately 30% of the solvent content) [22]. Apparently, the A_P value we

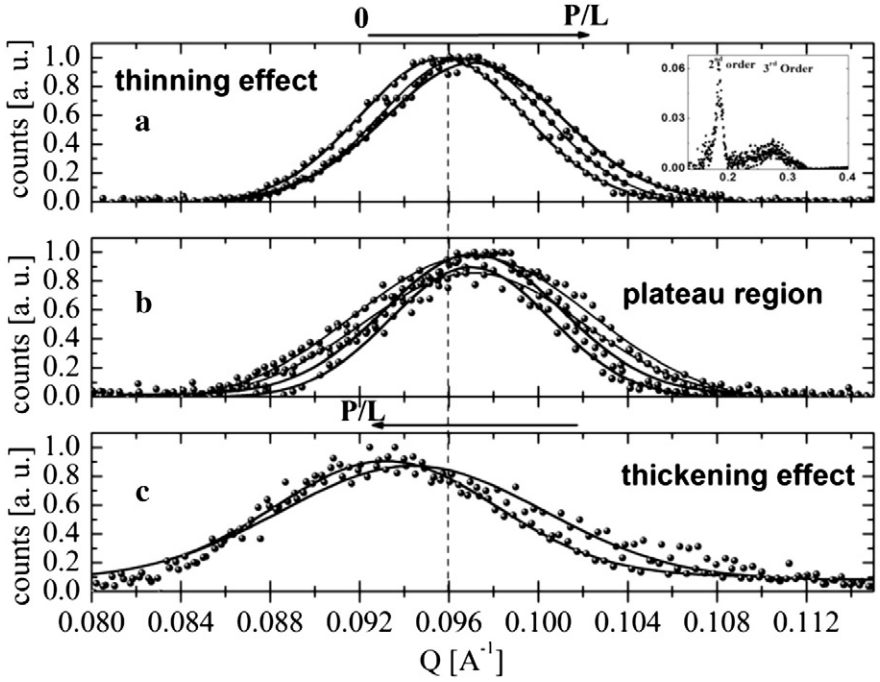

Fig. 2. First order Bragg peaks in reciprocal space of Ala-DPPC on silicon support at different values of *P*/*L* molar ratios, 25 °C and 100% RH are reported in scatter plot; corresponding best fit by Gaussian model in line plot. In the inset of the panel less intense peaks consistent with the second and third order Bragg peaks of the DPPC lamellar structure are shown. Panel a: The shift towards progressively higher mean *Q* values of the peaks with *P*/*L* increasing from 0 to 0.00625 (see the arrow), as reflecting a thinning effect of the periodical spacing of the samples. Panel b: For *P*/*L* ranging from 0.0125 to 0.0333 no significant change in the peaks position was observed. Panel c: The shift towards progressively lower mean *Q* values of the peaks corresponding to *P*/*L* of 0.05 and 0.1 (see the arrow), as reflecting a thickening effect of the periodical spacing of the samples.

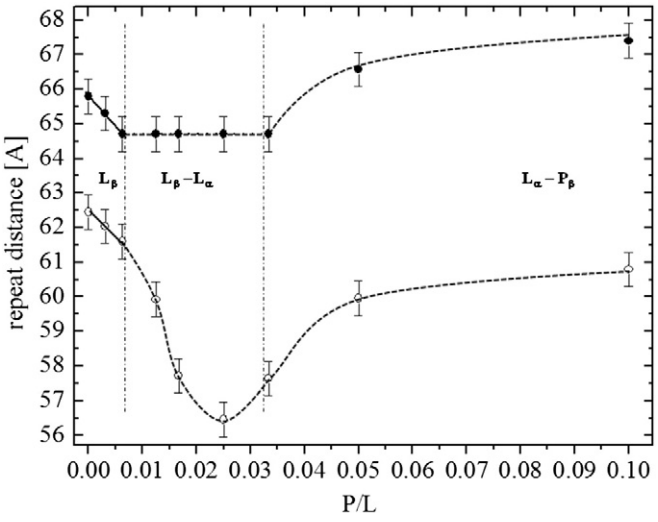

Fig. 3. Periodical spacings (repeated distance) as a function of *P/L* ratios of Ala-DPPC samples measured at 25 °C are plotted: for 50 (empty circles) and 100% RH. The plot is divided into three main regions depending on the suggested DPPC structural phase: the L_β one (linear fits in solid line), the L_β–L_α, and the L_α–P_β ones for the *P/L* ranges where lipid phase transitions are considered (interpolated curves as guide for the eyes in dotted lines).

found was independent from the hydration treatment of the Ala-DPPC membrane. This could mean that at 25 °C, the PC heads of DPPC binding to Ala had a greater affinity compared with the water molecules, so that during the process of sample hydration, the PC-Ala binding regions could not be interleaved by water. Accordingly, it was previously hypothesised that some water molecules are released from the headgroup region of the PC lipids when the peptide was embedded, estimating that each Ala binding causes the release of 8–13 water molecules [22].

It was also worth noting that having found agreement between the elastic model [22] and the linear thinning of gel-crystalline DPPC membranes, herein evidenced, no lipid structural phase transitions should therefore be induced by such small Ala concentrations. In contrast, when proceeding to higher Ala concentrations (0.00625 ÷ 0.0250, *P/L*), the change of *d vs. P/L* in the samples was not linear anymore (Fig. 3), exhibiting different trends, depending on the hydration treatment. Specifically, on the hypo-hydrated samples, the rate of reduction of *d* with *P/L* became progressively higher (the corresponding line profile in Fig. 3 loses linearity and becomes comparatively steeper), and the *w* values increased as well, until *d* approached the minimum value of 56.5 Å. This value was very similar to that estimated for the low-hydrated L_α DPPC assembly [34]. As judged from the analogy of the repeat distance, one of the main reasons for this phenomenon might be Ala's ability to trigger the gel–liquid crystalline phase transitions in the DPPC membrane.

DSC, AFM and computational analyses [31,32,24,53] previously reported on the influence of the peptides on the phase behaviour of PC membranes. DSC measurements [32] showed that the melting of peptide coupled lipids occurred at lower temperatures than did the pure phospholipid membrane. The peptide-induced softening of the lipid membrane was in conformity with Monte Carlo simulation studies that revealed increased fluctuations of the lipid phase, according to the gel–liquid crystalline structural transition near the clusters of gramicidin peptides [53]. The latter prediction may correspond to an increased disordering of the lipid structure, which was consistent to the comparatively larger Bragg peaks we observed. Such a supposed phase transition was expected to be completed at *P/L* of ~0.0250, with the latter being located at the respective *d* minimum point (Fig. 3), and the corresponding Bragg peaks *w* becoming comparatively narrower, accordingly (see Table 1). In this frame, our measurements provided novel experimental support for considering the existence of a range of *P/L* where a non-negligible perturbation of the equilibrium lipid-phase structure of low hydrated Ala-DPPC membrane might occur.

It was also worth noting that in the latter case, the clear discrepancy between the elastic model and the EDXD data reported herein did not allow us to derive information regarding how the peptide was configured within the DPPC bilayers.

From a free energy point of view, because of the lipid melting, the reduction of the DPPC membrane thickness might favour the conformational switching of Ala helices to form transverse membrane pores (see also Section 3), where a hydrophobic mismatch around the predominantly hydrophobic surface of the peptide molecules was reduced (and therefore, the free energy of the system was minimised). In this scenario, the presence of water was expected to contribute further in maximising the hydrophobic interactions between the peptide and the acyl chains of the lipids, and then to stabilise the peptide pore configuration. In the literature, AFM images [32] have indeed demonstrated that the physical behaviour of the lipid membrane in the water environment was altered in the vicinity of the Ala-induced pores, where the height profile in these areas corresponded to the thickness of the DPPC membranes in the fluid phase.

Along this line, Fig. 3 showed that the *d* value of the respective fully-hydrated samples (0.00625 ÷ 0.03333, *P/L*) increased to the common equilibrium value of 64.7 Å. This was consistent with the lattice constant of fully hydrated DPPC membranes just above the transition point (see also Supplementary Data, Fig. S2). With regards to the elastic model [22] (Section 3) and to the above-mentioned considerations, due to the sample hydration process, it might mean that an increasing fraction of peptides reorients in a perpendicular configuration embedded in liquid-crystalline DPPC bilayers. In such conditions, the bilayer thickness of several liquid crystalline phospholipids containing Ala was expected to level off after a $(P/L)^*$, depending on the lipid composition [18]. Notice, however, that the corresponding $(P/L)^*$ of 0.00625 that was carried out for DPPC was consistent with the ones reported for other liquid-crystalline PC structures previously investigated [18,40].

As seen in the third region of Fig. 3, the *d* value of the samples measured at both 50 and 100% RH was predicted to improve (substantially with the same growth rate), leading towards 60.8 Å and 67.4 Å, respectively for $P/L \approx 0.1$. Notably, the latter value overcame the value of the pure DPPC system, in striking agreement with the results reported for P_β of the oriented DPPC film [47]. Thus, an appealing hypothesis in this case concerns the possibility that structural phase transitions of the DPPC bilayer might be the main cause of such unexpected increase in the repeat distance we observed. Indeed, a comparative thickening of the Ala-DPPC structure, at a similar peptide concentration, was also reported using freeze–fracture cryo-scanning electron microscopy measurements [33]. The phenomenology was interpreted as the ability of Ala to change the morphology of DPPC bilayers in favour of a P_β-like structure [33].

In giving further consistency to the similarities we observed in periodical spacing between Ala-DPPC structure existing at room temperature and thermotropic mesophases exhibited by bare DPPC membrane, when all of the other conditions were equal, we performed EDXD measurements on the silicon supported DPPC membrane at varying temperatures (from 25 °C to 60 °C). Here, we focused on the fully hydrated structure (100%, RH), as it was believed that the mesophase transition L_β–P_β cannot be exhibited within a poorly hydrated DPPC membrane. The corresponding *d* values of the fully hydrated sample are plotted as a function of temperature in Fig. S2.

As expected [47,54], *d* of L_β DPPC film increased with the temperature until ~35 °C, at which time, *d* assumed the maximum value of 67.4 Å. At this temperature, a L_α–P_β transition (of fully hydrated DPPC membranes) was expected to occur. We would also stress that above ~35 °C, the values of *d* parameter of DPPC progressively decreased, likely due to the loss of water content, and at 50 °C (up to the gel to liquid-

crystalline transition point), it became similar to that observed for Ala-DPPC at 100% RH. Along the same lines, preliminary measurements on the sample $P/L = 0.025$, where the structural phase transition was supposed to be completed also under low hydration conditions (50% RH), there was no evidence of L_β–L_α structural phase transition in the working temperature range of 25–60 °C. These results seem to indicate that the presence of Ala at 25 °C allowed for the simulation of a thermotropic structural change during the L_β DPPC phase.

Despite this, some aspects remain unexplained and deserve at least some interpretation. In particular, it was worth noting that, separately from the thermotropic behaviour of DPPC, the increase of the concentration of the peptide in the lipid membrane first led to the L_β–L_α transition, followed by an apparently anomalous L_α–P_β, which may have been triggered even in low levels of hydration of the lipid membrane. However, this was not surprising if we consider that the formation of zipped L_α domains coexisting within L_β was thought to be an essential step in driving the dynamics of relaxation from L_β to stable P_β on DPPC bilayer [34]. As evidenced by time-resolved X-ray small and wide-angle diffraction, the formation of zipped liquid-crystalline domains coexisting within the gel-crystalline phase of the DPPC bilayer was an essential step in driving the dynamics of relaxation in a stable ripple structure [34].

Overall, this EDXD study reported on solid supported Ala-DPPC membranes and provided the range of P/L where the change of d was supported by the elastic model; moreover, evidencing the experimental traits whose understanding, instead, might require the formulation of a more complex model, including the contributions to free energy, due to the structural mesophase transition of the Ala-DPPC membrane.

The existence of correlated biological effects of Ala represents the other crucial aspect, which deserves to be investigated.

4.2. In vitro cytotoxicity and morphological screening of Ala

The viability of the *HeLa* cell line exposed to Ala at different concentrations (ranging from 50 to 4×10^{-4} μg/ml) for 2, 6 and 20 h, was evaluated by the MTT assay. The antiproliferative activity after treatments for 2, 6 and 20 h is reported in Fig. 4a, b and c, respectively.

As shown in the bar charts, Ala inhibits the viability of *HeLa* cells in a dose-dependent manner. More specifically, high concentrations of the compound induced a severe decrease in cell viability for each treatment procedure. At very low concentrations of Ala we instead observed a slight increase in cell viability rates. The latter effect was evident after 20 h of incubation with 0.0016 μg/ml of Ala (Fig. 4c).

The results of the cytotoxic activity *in vitro* were also expressed as IC50, the dose of the compound (μg/ml) that inhibits the proliferation rate of the tumour cells by 50%, as compared to the untreated cells (control). The average IC50 values of Ala against this cancer cell line were 7.5 μg/ml after 2 h, 4 μg/ml after 6 h and 0.3 μg/ml after 20 h respectively.

To evaluate the effect of Ala on the cell membrane, we carried out a morphological examination of the cell line using light microscopy. Selected images of untreated (control) and treated *HeLa* cells are presented in Fig. 5. As shown in Fig. 5 (images a and f), untreated cells (control) were confluent, attached firmly to the substratum with random orientations, displaying unaffected morphology without membrane damage.

Fig. 5 (images b–e) shows cells treated for 2 h. Treatments starting from 5.0 μg/ml of Ala induced significant and progressive retraction and consequent disruption of the plasma membrane in a dose/dependent manner (Fig. 5c and d). Administration of 50 μg/ml of Ala resulted in cellular membrane dissolution (Fig. 5e).

Representative images of *HeLa* cells morphology that underwent 20 h of Ala incubation are found in Fig. 5 (images g–m). Following treatment with 0.06 μg/ml, cells partially retained their normal shapes and had morphological alteration (Fig. 5h). They retracted and detached from the substratum after the treatment increased to 0.25 μg/ml,

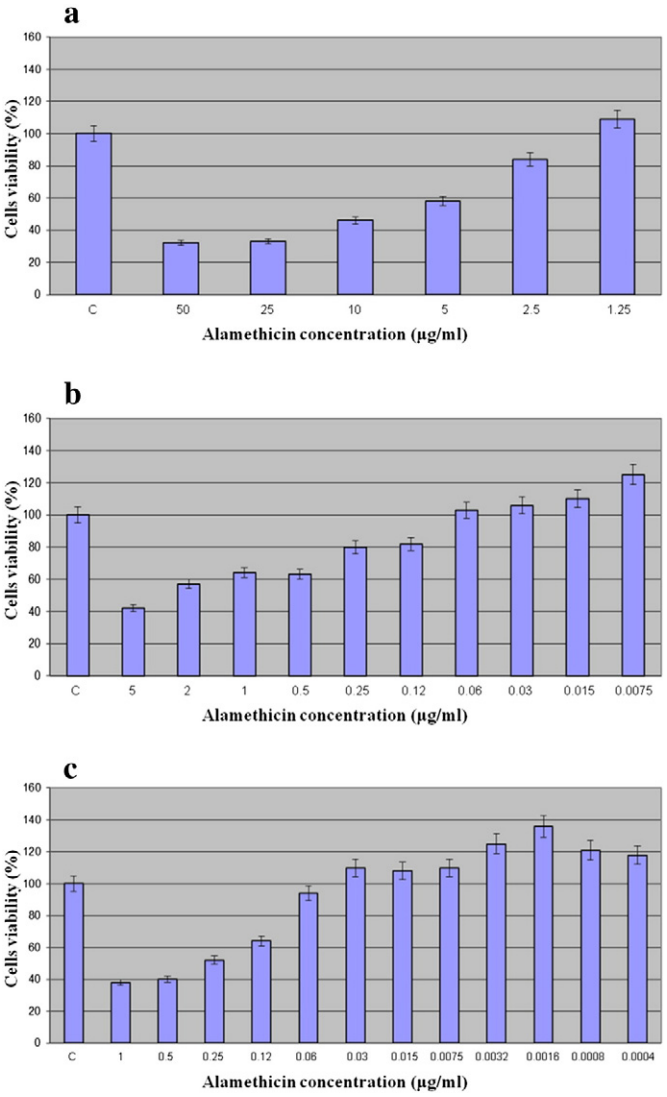

Fig. 4. Effects of the antimicrobial peptide Ala on the viability of *HeLa* cells following 2 (a), 6 (b) and 20 h (c) of incubation, using the MTT assay. Tumour cells were exposed to different concentrations of the compound (ranging from 50 to 4×10^{-4} μg/ml) or fresh culture medium as control. The results represent the mean percentage ± standard deviation.

partially losing their viability (Fig. 5i). Cells treated with the highest doses (0.5 and 1.0 μg/ml) showed severe retraction and more rounding (Fig. 5l and m). The overall observations indicated that the decreased viability of *HeLa* cultures undergoing treatment with Ala was related to the destruction of the membrane's integrity.

Our results were consistent with those of Paredes-Gamero et al. [4]. Using light microscopy, they observed that high concentrations of four β-hairpin antimicrobial peptides (gomesin, protegrin, tachyplesin and polyphemusin II), as well as some of their linear analogues, also induced rapid membrane disruption in erythro-leukaemia cell line with diverse characteristics: gomesin, tachyplesin, Lin-tachyplesin, polyphemusin II and its linear analogue led to a substantial alteration and total disruption of the cell membrane. Protegrin produced rounding and swelling of cells, typical in necrotic cell death [4]. Moreover, in a recent electron microscopy study [5], it was observed that after 1 h of incubation of various concentrations of temporin-1CEa in two breast cancer cell lines, the cell membranes were shrivelled, invaginated and disrupted. This damage resulted in irreversible cytolysis, and finally, in cell death [5]. Finally, Steinstraesser and colleagues [6], in an experiment carried out on the human synovial sarcoma cell line, observed that after a short incubation time of 30 min with the [D]-K3H3L9 peptide, the cell membrane was

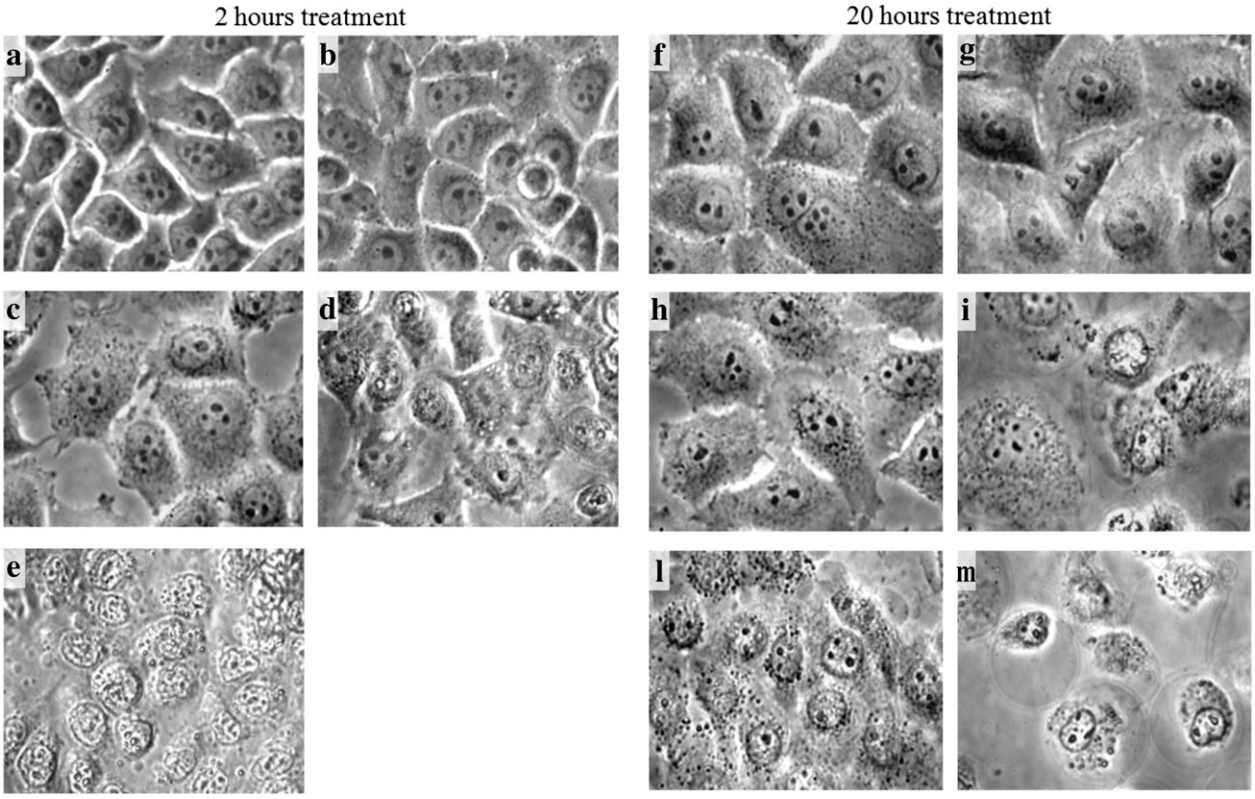

Fig. 5. Morphological changes in *HeLa* cells treated with the antimicrobial peptide Ala are shown. On the left side, the images show *HeLa* cells treated for 2 h with fresh culture media as control (a), and with the Ala doses: 1.25 μg/ml (b), 5.0 μg/ml (c), 10 μg/ml (d), and 50 μg/ml (e). On the right side, the images show *HeLa* cells treated for 20 h with fresh culture media as control (f), and with the Ala doses: 0.003 μg/ml (g), 0.06 μg/ml (h), 0.25 μg/ml (i), 0.5 Ala μg/ml (l), and 1.0 μg/ml (m). Untreated cells (control) show a normal smooth surface, while cells treated with Ala reveal a disrupted cell membrane. Each image was acquired at 40× objective magnification.

affected and began to lose its integrity. After 24 h, the plasma membrane was completely destroyed.

Beside the cytotoxic effects of such peptides, also an increased proliferation and differentiation cell processes were recently demonstrated [55,56]. In particular, some researchers in an experiment designed to understand the role of the human β-defensins (hBDs) in cellular stimulation, have demonstrated that hBD-2 increased the osteoblast-like MG63 cell proliferation [56]. Such an increase, equal to 123%, was significant at a dose of 50 nM and an incubation time of 24 h [56], which was striking similar to what we observed with our results shown in Fig. 4c.

4.3. Correspondence between Ala effects on DPPC membrane and in vitro

As explained in Sections 3 and 4.2, Ala might exert an antimicrobial/cytotoxic activity due to the interaction of the peptide with the membrane. It was originally thought that the cytotoxic effects were triggered by morphological changes at the level of lipids composing the plasma membrane [1–3]. For this reason, it made sense to analyse whether there was a correspondence between the doses of Ala where the morphological/cytotoxic effects took place *in vitro* and the *P*/*L* values at which the structural findings were achieved on a membrane lipid model, according to Sections 4.1 and 4.2 respectively.

In order to make this comparison, we calculated the ratio of *P*/*L* that was equivalent to each dose of Ala used for the *in vitro* experiments. A rough estimate of the total amount of lipids equivalent to the cells [57] in a single well was ~0.5 μg. From this, it was easy to calculate that a *P*/*L* ratio equals to 1 corresponds with ~1.3 μg of Ala per cell well. Due to the strong affinity of the Ala to the lipid membrane, as well as to its low affinity to water, we assumed that in practice, the whole peptide amount was adsorbed on the plasma membrane of *HeLa* [58]. The values of the concentrations of Ala used for viability tests, in terms of equivalent *P*/*L* molar ratios, are shown in Table S1 of the Supplementary Data.

As outlined in Fig. 6, the comparison reveals a clear correspondence between the values of *P*/*L* where a modulation in vertical ordering of the DPPC model membrane occurs and the values at which Ala exerts its cytotoxic activity on *HeLa*. Specifically, we found that $P/L = 0.00313$, where Ala was predicted to adsorb parallel to the surface of the DPPC membrane model causing a thinning of the lipid bilayer thickness,

P/L (Ala/DPPC)	*In vitro* treatment		
0.00313	20 hours		
0.00625		6 hours	
0.01250			
0.01667			
0.02500			
0.03333			
0.05000			2 hours
0.1			
1			

Fig. 6. Overlapping of *P*/*L* regions at which both vertical ordering changes on Ala-DPPC and times at which Ala significantly affects *HeLa* viability.

and, in turn, of the *d* parameter, corresponded to slightly above the *in vitro* threshold dose of 0.06 μg/ml of Ala with regards to the changes in viability and morphology documented after 20 h of treatment. In this respect, we would stress that existing reports [31,46] discussed the importance of the lipid bilayer spacing, whose small variations might effectively interfere with the proper transmembrane protein sorting and biological functions of the cell plasma membranes (see also Section 3). At 6 h of treatment, the cytotoxic effect and the structural variations of the plasma membrane overlapped at the *P*/*L* of 0.00625. Consistent with the lipid membrane models, from this value the peptide would also be able to affect the cell permeability by forming non-specific pores on the cell plasma membrane, together with possible alterations of the corresponding lipid phase.

Finally, the range of Ala doses between 1.25 μg/ml and 25 μg/ml, where the strong decrease of the *HeLa* viability was observed after 2 h of treatment, intersected with the *P*/*L* values that ranged from 0.05 to 1. In the latter *P*/*L* range, the pore-forming Ala aggregates also induced a significant increase of *d* in the Ala-DPPC multilayers (which could hide a lipid structural transition), or, for the higher *P*/*L* value, even induced a membrane detergent effect, which was consistent with the *HeLa* plasma membrane dissolution reported in Fig. 5e.

The results of the comparison reported above could have some biomedical relevance if we consider that the lecithin DPPC was of major importance for the lipid raft formation [29]. Indeed, the existence of such liquid-ordered lipid domains was recently highlighted in much of the plasma membrane in the live *HeLa* cells [59]. The presence of such lipid rafts was believed to be relevant in various tumour cellular functions, including the regulation of cell adhesion and protein-mediated membrane signalling [59]. In this respect, the search for any selective cytotoxic activity of Ala and of other antimicrobial peptides, with respect to the neoplastic status of cells, might be important and deserves a dedicated study.

Nevertheless, some literature that focused on different systems demonstrated that the alteration of wild-type cytoplasmic membranes was only a part of the mechanism through which the antimicrobial peptides could cause the death of cells [4,5,7–9]. In such cases (*i.e.* Lactoferricin B, temporin-1CEa and β-hairpin peptides), the formation of transmembrane pores allowed the peptide to enter the cytoplasmic compartment of the cell, and thereby to co-localise in the cell organelles [7,8]. Here, they promoted cell death *via* an apoptotic process that involved the sequential generation of reactive oxygen species, the loss of mitochondrial membrane potential, and the activation of the caspase cascade [9]. They also possibly affected the intracellular calcium mechanisms [4,5]. In light of the latter evidence, it is important to emphasise here that the reliability and usefulness in correlating cytotoxicity to ordering variations on lipid membrane models was necessary to further verify, in the specific case under examination, that the causes of cell mortality effectively coincided with the morphological and structural alteration of the plasma membrane.

5. Conclusions

The analysis of the samples of Ala-DPPC performed at 50 and 100% RH conditions using a wide range of *P*/*L* molar ratios, together with the availability of EDXD, allowed us to provide a more comprehensive knowledge concerning the *d* parameter trends as a function of *P*/*L*. The results were then used to provide information regarding the cytotoxic behaviour we observed *in vitro*.

The diffraction data were consistent with the previous reports on the occurrence of a threshold *P*/*L* value with respect to the variation of *d* with *P*/*L* on the Ala-DPPC multilayer reflecting what was exhibited by the bilayer thickness, depending on the conformation of the peptide inserted within. The respective linear decrease and plateau regions of the *d*-trends reported here were consistent with the elastic model, which assumed that the peptide was oriented parallel to the lipid membrane surface and in the trans-membrane pore configuration, respectively.

Our results go beyond this by highlighting the *P*/*L* values where the variations of *d* of the Ala-DPPC membrane fell outside the behaviour of the vertical ordering predicted by the elastic model that had been suggested after studying other phospholipids. In particular, the revealed non-linear decrease of *d* with a *P*/*L* that had been reduced to a critical point, as well as the increase of *d* at higher *P*/*L* values, depending on hydration, demonstrated some striking similarity to the thermo-lyotropic structural changes exhibited by DPPC. Along this line, we are confident that forthcoming detailed thermo-lyotropic investigations will be useful in better clarifying whether some phase transitions in the solid-supported DPPC could effectively occur with the use of Ala.

While the EDXD experiments were performed on a highly simplified model system, we highlighted a noteworthy correspondence of both the order of magnitude and the range of values of Ala concentrations where the cytotoxic effect took place. In particular, we demonstrated the existence of an overlapping region between the range of *P*/*L* values that corresponded to the changes on the vertical spacing of the solid supported lipid bilayers and the values where the effects on the plasma membrane, as well as on the cell's viability, occurred. Hence, it actually seems possible to calibrate the structural findings that are then easily monitored using a membrane model to predict the Ala doses necessary to trigger cell death through plasma membrane alterations.

Transparency document

The Transparency document associated with this article can be found, in the online version.

Acknowledgements

We thank Dr J. Generosi and Dr. D. Panichelli for their helpful discussions and excellent experimental support, and Dr. S. Belardinelli for his qualified assistance in the sample preparation.

Appendix A. Supplementary data

Supplementary data to this article can be found online at http://dx.doi.org/10.1016/j.bbagen.2015.01.006.

References

[1] C.D. Fjell, J.A. Hiss, R.E. Hancock, G. Schneider, Nat. Rev. Drug Discov. 11 (2012) 37.
[2] C. Auvynet, Y. Rosenstein, FEBS J. 276 (2009) 6497.
[3] M.T. Lee, W.C. Hung, F.Y. Chen, H.W. Huang, Proc. Natl. Acad. Sci. U. S. A. 105 (2008) 5087.
[4] E.J. Paredes-Gamero, M.N. Martins, F.A. Cappabianco, J.S. Ide, A. Miranda, Biochim. Biophys. Acta 1820 (2012) 1062.
[5] C. Wang, L.-L. Tian, S. Li, H.-B. Li, Y. Zhou, H. Wang, Q.-Z. Yang, L.-J. Ma, D.-J. Shang, PLoS ONE 8 (2013) 1.
[6] L. Steinstraesser, J. Hauk, C. Schubert, S. Al-Benna, I. Stricker, H. Hatt, Y. Shai, H.-U. Steinaul, F. Jacobsen, PLoS ONE 6 (2011) 1.
[7] J.S. Mader, A. Richardson, J. Salsman, D. Top, R. de Antueno, R. Duncan, D.W. Hoskin, Exp. Cell Res. 313 (2007) 2634.
[8] L.T. Eliassen, G. Berge, A. Leknessund, M. Wikman, I. Lindin, C. Løkke, F. Ponthan, J.I. Johnsen, B. Sveinbjørnsson, P. Kogner, T. Flægstad, Ø. Rekdal, Int. J. Cancer 119 (2006) 493.
[9] J.S. Mader, J. Salsman, D.M. Conrad, D.W. Hoskin, Mol. Cancer Ther. 4 (2005) 612.
[10] P. Nicolas, FEBS J. 276 (2009) 6483.
[11] R. Pignatello, T. Musumeci, L. Basile, C. Carbone, G. Puglisi, J. Pharm. Bioallied Sci. 3 (2011) 4.
[12] F. Bordi, C. Cametti, C. Di Venanzio, S. Sennato, S. Zuzzi, Colloids Surf. B 61 (2008) 304.
[13] F. Domenici, C. Castellano, A. Congiu, G. Pompeo, R. Felici, Appl. Phys. Lett. 92 (2008) 193901.
[14] M. Tanaka, E. Sackmann, Nature 437 (2005) 656.
[15] T. Salditt, Curr. Opin. Struct. Biol. 13 (2003) 467.
[16] E. Sackmann, Science 271 (1996) 43.
[17] M. Diociaiuti, F. Bordi, A. Motta, A. Carosi, A. Molinari, G. Arancia, C. Coluzza, Biophys. J. 82 (2002) 3198.
[18] F. Domenici, D. Panichelli, A. Congiu Castellano, Colloids Surf. B 69 (2009) 216.
[19] R.A. Vaucher, M.L. Teixeira, A. Brandelli, Curr. Microbiol. 60 (2010) 1.

[20] B. Leitgeb, A. Szekeres, L. Manczinger, C. Vágvölgyi, L. Kredics, Chem. Biodivers. 4 (2007) 1027.
[21] K.A. Brogden, Nat. Rev. Microbiol. 3 (2005) 238.
[22] M.-T. Lee, F.-Y. Chen, H.W. Huang, Biochem. J. 43 (2004) 3590.
[23] F.-Y. Chen, M.-T. Lee, H.W. Huang, Biophys. J. 82 (2002) 908.
[24] K. He, S.J. Ludtke, D.L. Worcester, H.W. Huang, Biochem. J. 34 (1995) 15614.
[25] R.J. Taylor, R. de Levie, Biophys. J. 59 (1991) 873.
[26] V. Rizzo, S. Stankowski, S. Schwartz, Biochem. J. 126 (1987) 2751.
[27] C. Li, T. Salditt, Biophys. J. 91 (2006) 3285.
[28] L. Yang, T.A. Harroun, T.M. Weiss, L. Ding, H.W. Huang, Biophys. J. 81 (2001) 1475.
[29] D. Hakobyan, A. Heuer, PLoS ONE 9 (2014) 1.
[30] L.N. Okoro, Eur. Chem. Bull. 2 (2013) 107.
[31] V. Oliynyk, M. Jäger, T. Heimburg, V. Bucki, U. Kaatze, Biophys. Chem. 134 (2008) 168.
[32] V. Oliynyk, U. Kaatze, T. Heimburg, Biochim. Biophys. Acta 1768 (2007) 236.
[33] T.J. McIntosh, H.P. Ting-Beall, G. Zampighi, Biochim. Biophys. Acta 685 (1982) 51.
[34] M. Rappolt, G. Pabst, G. Rapp, M. Kriechbaum, H. Amenitsch, C. Krenn, S. Bernstorff, P. Laggner, Eur. Biophys. J. 29 (2000) 125.
[35] V.I. Gordeliy, M.A. Kiselev, P. Lesieur, A.V. Pole, J. Teixeira, Biophys. J. 75 (1998) 2343.
[36] M. Seul, M.J. Sammon, Thin Solid Films 185 (1990) 287.
[37] F. Domenici, C. Castellano, F. Dell'Unto, A. Congiu, Colloids Surf. B 95 (2012) 170.
[38] A. Congiu, D. Pozzi, C. Esposito, C. Castellano, G. Mossa, Colloids Surf. B 36 (2004) 43.
[39] L.R. Opsahl, W.W. Webb, Biophys. J. 66 (1994) 71.
[40] F.Y. Chen, M.T. Lee, H.W. Huang, Biophys. J. 84 (2003) 3751.
[41] T.A. Harroun, W.T. Heller, T.M. Weiss, L. Yang, H.W. Huang, Biophys. J. 76 (1999) 937.
[42] T.A. Harroun, W.T. Heller, T.M. Weiss, L. Yang, H.W. Huang, Biophys. J. 76 (1999) 3176.
[43] M.R.R. De Planque, D.V. Greathouse, R.E. Koeppell, H. Schaefer, D. Marsh, J.A. Killian, Biochem. J. 37 (1998) 9333.
[44] O.G. Mouritsen, M. Bloom, Biophys. J. 46 (1984) 141.
[45] J.A. Killianl, M.R.R. de Planque, P.C.A. van der Wel, I. Salemink, B. de Kniijff, D.V. Greathonse, R.E. Koeppe, Pure Appl. Chem. 70 (1998) 75.
[46] O.S. Andersen, R.E. Koeppe, Annu. Rev. Biophys. Biomol. Struct. 36 (2007) 107.
[47] J. Katsaras, S. Tristram-Nagle, Y. Liu, R.L. Headrick, E. Fontes, P.C. Mason, J.F. Nagle, Phys. Rev. 61 (2000) 5668.
[48] M. Bachar, O.M. Becker, J. Chem. Phys. 111 (1999) 8672.
[49] M. Bachar, O.M. Becker, Bilayer Biophys. J. 78 (2000) 1359.
[50] K. Gawrisch, J.A. Barry, L.L. Holte, T. Sinnwell, L.D. Bergelson, J.A. Ferretti, Mol. Membr. Biol. 12 (1995) 83.
[51] F. Foglia, D.J. Barlow, F.C. Szoka, Z. Huang, S.E. Rogers, M.J. Lawrence, Langmuir 27 (2011) 8275.
[52] P.J. Quinn, H. Takahashi, I. Hatta, Biophys. J. 68 (1995) 1382.
[53] V.P. Ivanova, I.M. Makarov, T.E. Schäffer, T. Heimburg, Biophys. J. 84 (2003) 2427.
[54] M.P. Hentschel, F. Rustichelli, Phys. Rev. Lett. 66 (1991) 903.
[55] M. Pushpanathan, P. Gunasekaran, J. Rajendhran, Int. J. Pept. 2013 (2013) 1.
[56] D. Kraus, J. Deschner, A. Jäger, M. Wenghoefer, S. Bayer, S. Jepsen, J.P. Allam, N. Novak, R. Meyer, J. Winter, J. Cell. Physiol. 227 (2012) 994.
[57] S. Johnsen, T. Stokke, H. Prydz, J. Cell Biol. 63 (1974) 357.
[58] S. Stankowski, G. Schwarz, FEBS Lett. 250 (1989) 556.
[59] D.M. Owen, D.J. Williamson, A. Magenau, K. Gaus, Nat. Commun. 3 (2012) 1256.